Supporting Information

N,P-coordinated fullerene-like carbon nanostructures with dual active centers toward high-efficient multi-functional electrocatalysis for CO_2 RR, ORR and Zn-air battery

Xiaoyi Xue,[†,a] Hui Yang, [†,b] Tao Yang, [†,b,c] Pengfei Yuan,[d] Qing Li,[b] Shichun Mu,[e] Xiaoli Zheng,[a] Lifeng Chi,[b] Jia Zhu,[,c] Yanguang Li,[*,b] Jianan Zhang[*,a] and Qun Xu[a]*

[a] College of Materials Science and Engineering, Zhengzhou University, Zhengzhou 450001, P. R. China. *E-mail: zjn@zzu.edu.cn

[b] Institute of Functional Nano and Soft Materials (FUNSOM), Jiangsu Key Laboratory for Carbon-Based Functional Materials and Devices, Soochow University, Suzhou 215123, China. *E-mail: yanguang@suda.edu.cn

[c] Key Laboratory of Theoretical and Computational Photochemistry, Ministry of Education, College of Chemistry, Beijing Normal University, Beijing 100875, China. *E-mail: zhu.jia@bnu.edu.cn

[d] International Joint Research Laboratory for Quantum Functional Materials of Henan Province, and School of Physics and Engineering Zhengzhou University, Zhengzhou 450001, P. R. China

[e] State Key Laboratory of Advanced Technology for Materials Synthesis and Processing, Wuhan University of Technology, Wuhan 430070, P. R. China

[†]These authors contributed equally to this work.

1. Experimental Section

Electrocatalytic CO_2 reduction measurement. Electrochemical experiments were implemented in a designed H-shaped electrochemical cell with two compartments separated by anion-exchange membrane. Each compartment contained ~30 mL electrolyte (0.5 M $NaHCO_3$) and the headspace was ~25 mL. The working electrode was carbon fiber paper (Fuel Cell). The saturated calomel electrode (SCE) and a graphite rod served as reference and the counter electrodes, respectively. In a typical preparation of the working electrode, 1 mg of sample and 0.5 mg of Ketjenblack carbon black were dispersed in a mixture of 6 μL of 5 wt % Nafion solution and 250 μL of ethanol to get a homogeneous ink after 40 min of sonication. Then the catalyst ink was loaded onto a hydrophobic carbon fiber paper with an area of 1 cm^2 (1 cm x 1 cm). Before electrochemical reactions, the electrolyte was purged with N_2 or CO_2 to get N_2-saturated $NaHCO_3$ (pH=8.4) or CO_2-saturated $NaHCO_3$ (pH=7.4). Cyclic voltammetry and polarization curves were carried out with a scan rate of 10 mV s^{-1} by CHI 660E potentiostate. All potentials were iR-corrected and converted to the RHE scale ($E_{RHE} = E_{SCE} + 0.241\ V + 0.0591\ V \times pH$).

In order to analyze the reduction production and calculate their Faradaic efficiency, electrolysis was performed at a few selected potentials for 1-5 h. During the electrolysis, the electrolyte was bubbled with a CO_2 flow of 20 sccm to keep the saturation. Then the CO_2 flow was vented to a gas chromatograph (GC, Aligent 7890B) equipped with a molecular sieve 5A and two porapak Q columns. The concentration of H_2 was quantified by a thermal conductivity detector (TCD), and the concentration of CO was analyzed by a flame ionization detector (FID) with a methanizer. The Faradic efficiency of gas product was calculated as below:

$$\boldsymbol{FE}(\%) = \frac{\boldsymbol{Q_{co}}}{\boldsymbol{Q_{tot}}} \times \mathbf{100}\% = \frac{\left(\frac{\boldsymbol{x}}{\mathbf{24000}\ \boldsymbol{cm^3/mol}}\right) \times \boldsymbol{N} \times \boldsymbol{F}}{\boldsymbol{j} \times \left(\frac{\mathbf{60}\ \boldsymbol{s/min}}{\boldsymbol{v}}\right)} \times\ \mathbf{100}\%$$

Where $\boldsymbol{x}$ is the concentration of H_2 or CO in the 1 mL of sample loop based on the calibration of the GC with a standard gas, $\boldsymbol{v}$ is the flow rate of CO_2 (20 sccm). $\boldsymbol{N}$ (=2) is the electron that needed to form a molecule of H_2 or CO. $\boldsymbol{F}$ is the Faradaic constant (96485 C mol^{-1}), and *j* is the recorded current.

Electrocatalytic oxygen reduction reaction measurement. Electrochemical experiments were conducted on a CHI760E electrochemical workstation (CH Instrument Co., USA). CV, RDE, and RRDE

measurements (Pine Research Instrument, USA) were conducted using a standard three-electrode system. All the measurements were carried out at room temperature. For the preparation of working electrode, 5 mg catalyst dispersed dispersed in 480 μL of DI water/isopropyl alcohol (v/v~3:7)/20 μL Nafion (20 wt.%) solution, under sonication for 1 h to form a homogeneous catalyst ink. Then, 2 μL of this catalyst ink was pipetted onto the glassy carbon (GC) electrode (0.19625 cm^2), and dried at room temperature. The catalyst loading for the prepared catalyst on the GC electrode and commercial Pt/C (20 wt%) was 0.10 mg cm^{-2}. A typical three-electrode system was employed, using a glass carbon RDE covered by catalyst as working electrode, a platinum wire as counter electrode, and an Ag/AgCl electrode (saturated with KCl) as reference electrode. All potentials in this study were converted to potential *vs*. reversible hydrogen electrode (RHE) according to the equation ($E_{RHE} = E_{Ag/AgCl} + 0.197 + 0.059 \times pH$). As for ORR experiment, O_2 was bubbled for 30 min prior to the test and maintained in the headspace of the electrolyte. throughout the testing process. The working electrode was scanned cathodically at a rate of 5 mV s^{-1} with varying rotating speed from 400 to 2250 rpm in O_2-saturated 0.1 M KOH aqueous solution. The electron transfer number per oxygen molecule for oxygen reduction can be determined on the basis of the Koutechy-Levich equation.[1]

$$\frac{1}{J} = \frac{1}{J_L} + \frac{1}{J_K} = \frac{1}{B\omega^{0.5}} + \frac{1}{J_K} \quad (1)$$

$$B = 0.62nFC_0(D_0)^{2/3}\nu^{-1/6} \quad (2)$$

$$J_K = nFkC_0 \quad (3)$$

Where J is the measured current density and is the electrode rotating rate (rad s^{-1}). B is determined from the slope of the Koutechy-Levich (K-L) plot based on Levich equation (2). J_L and J_K are the diffusion- and kinetic-limiting current densities, n is the transferred electron number, F is the Faraday constant (F = 96485 C mol^{-1}), C_0 is the O_2 concentration in the electrolyte ($C_0 = 1.26 \times 10^{-6}$ mol cm^{-3}), D_0 is the diffusion coefficient of O_2 ($D_0 = 1.93 \times 10^{-5}$ cm^2 s^{-1}), and v is the kinetic viscosity (v = 0.01009 cm^2 s^{-1}). The constant 0.62 is adopted when the rotation speed is expressed in rad s^{-1}. For OER experiments, the LSV curves were obtained at a scan rate of 5 mV s^{-1} with iR drop compensation. In order to obtain a stable current, the LSV data were collected at the second sweep. For the RRDE measurements, the disk electrode was scanned cathodically at a rate of 10 mV s^{-1} and the ring potential was kept at 1.5 V versus RHE. The peroxide percentage and the electron

transfer number (n) were determined by the following equations:[2]

$$HO_2^- \% = 200 \times \frac{I_R / N}{I_D + I_R / N} \quad (4)$$

$$n = 4 \times \frac{I_D}{I_D + I_R / N} \quad (5)$$

where I_d is disk current, I_r is ring current, and N is current collection efficiency of the Pt ring. N was determined to be 0.40.

Zinc-air battery tests. All Zn-air batteries were evaluated under ambient conditions. The catalyst ink recipe consists of 5.0 mg catalyst dispersed dispersed in 480 µL of DI water/isopropyl alcohol (v/v~3:7)/20 µL Nafion (5 wt.%) solution. The air electrode was prepared by uniformly coating the as-prepared catalyst ink onto carbon paper then drying it at 80 °C for 2 h. A Zn plate was used as the anode and catalysis loaded on carbon paper are used as cathodes. Both electrodes were assembled into a home-made Zn–air battery, and 6 M KOH aqueous solutions was used as the electrolyte.[3] The polarization curves were recorded by linear sweep voltammetry (5 mV s^{-1}, at room temperature) on a CHI 760D electrochemical platform.[4] The energy density was calculated based on the applied current (I), average discharge voltage (V), service time (t), and weight of zinc consumed (w_{zn}) as in the following equation:

$$\textbf{Energy density } (\textbf{W h kg}^{-1}) = \frac{\mathbf{I} * \mathbf{V} * \triangle \mathbf{t}}{\boldsymbol{w_{Zn}}}$$

The specific capacity was calculated according the equation below:

$$\textbf{specific capacity} (\textbf{mA h g}^{-1}) = \frac{\mathbf{I} * \triangle \mathbf{t}}{\boldsymbol{w_{Zn}}}$$

All-solid-state Zn–air battery assembly. A polished zinc foil (0.05 mm thickness) was used as anode. The gel polymer electrolyte was prepared as follow: polyvinyl alcohol (PVA, 5 g) was dissolved in 50 mL was added 18 M KOH (5 mL) and 2.5×10^{-3} M $Zn(CH_3OO)_2$ at 95 °C to form a homogeneous viscous solution, followed by casting on a glass disk to form a thin polymer film (thickness about 2 mm). The film was then freezed in a freezer at -20 °C about 2 h, and then keep at 0 °C temperature about 4 h. The film was thawed for 12 h before used. Then, the as-prepared catalyst film and zinc foil were placed on the two sides of PVA gel, followed by pressed Ni foam as current collector. The components were firmly pressed together by roll-pressing. No inert atmosphere or glove-box is required for the packaging.[5, 6]

2. Theoretical calculation

Methods and Models about CO_2 reduction. Electronic properties calculations were carried out using a projected augmented wave (PAW)[7] method with exchange-correlation interactions modeled by the PerdewBurke-Ernzerhof (PBE)[8] functional in the Vienna ab initio simulation package (VASP).[9, 10] A plane-wave energy cutoff 500 eV was used in all calculations after testing a series of different cutoff energies. The convergence threshold for geometry structural optimization was set as 0.01 eV $Å^{-1}$ and that for electronic structure iteration was set as 10^{-5} e V. A Gaussian smearing of 0.05 eV for the total energy calculations. The supercell method[11] was used to calculate N,P-doped fullerene and interaction with adsorbates, with a cell size of 20×20×20 $Å^3$. Gamma point was used for the geometry optimization and the total energy calculation. The Grimme's method (DFT-D3)[12] was applied during all calculations to correct the van der Waals interaction between atoms.

The free energy (G) of each species can be obtain by

$$\mathbf{G} = \boldsymbol{E_{total}} + \boldsymbol{E_{ZPE}} + \int \boldsymbol{C_P}\,\mathbf{dT} - \mathbf{TS}$$

where E_{total}, E_{ZPE}, C_{P}, S and T were total electronic energy, zero point energy, heat capacity, entropy, and system temperature (298.15K), respectively. For adsorbates, free energy were calculated by treating all 3N degrees of freedom of the adsorbate as vibrational without considering contributions from the substrate. All vibrations were treated in the harmonic oscillator approximation, and zero point energies, heat capacities, and entropies were calculated from these vibrations by standard methods. For molecules, those value were taken from NIST database. Because the gas-phase thermochemical reaction energies calculated with the PBE functional were inconsistent with experimental values,[13] after a series of gas-phase thermochemical reaction enthalpies testing to correct the reaction enthalpy , the total energy corrections for CO_2, CO, and HCOOH were +0.16, -0.27, and +0.17 eV, respectively. Based on the computational hydrogen electrode (CHE) model [14] the chemical potential of a couple of proton-electron at 0 V (vs RHE) is equal to one half of the chemical potential of hydrogen molecule at all temperature and 1.01×10^5 Pa. Adsorption energy E_{ads} is the indicate to evaluate the binding strength between adsorbates and substrate, which was defined as $E_{\text{ads}}=E_{\text{X}^*}-E_{\text{X}}-E_*$, where E_{X^*}, E_{X}, and E_* represent the total energy of the adsorption system, adsorbate, and the substrate, respectively. According to this definition,

the smaller E_{ads} means the stronger adsorption.

Methods and Models about ORR. First-Principles calculations were carried out within the density functional theory framework.[15] The projector-augmented wave (PAW) method[7] and the generalized gradient approximation (GGA)[16] for the exchange-correlation energy functional, as implemented in the Vienna *ab initio* simulation package (VASP)[9] were used. The GGA calculation was performed with the Perdew-Burke-Ernzerhof (PBE)[8] exchange-correlation potential. A plane-wave cutoff energy of 400 eV was used. All atoms were fully relaxed with a tolerance in total energy of 0.1 meV, and the forces on each atom were less than 0.02 eV/Å. The van der Walls interactions were included by DFT-D2[17] method. In all calculation, spin polarization was included.

The ORR reaction happened on N, P co-doped C60 and graphene was calculated. For N, P co-doped C60, a 20x20x20 $Å^3$ supercell was used, and only gamma point was used in this calculation. For N, P co-doped graphene, a 5x5 supercell (12.34x12.34 $Å^2$), and a 2x2x1 K-points was used, respectively. In both cases, the N and P coordinate type was the same. For each case, three different active sites were considersied: N atom, C atom linked with N and C atom linked with P.

3. Supplementary Figures and Tables

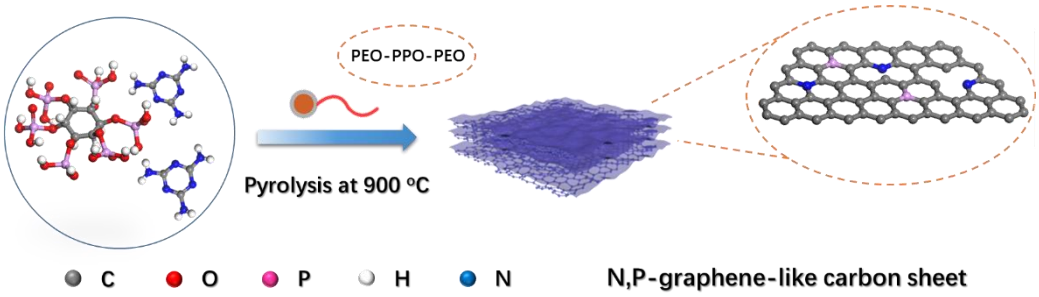

Scheme S1. The illustration of the synthetic protocol of N,P-FG.

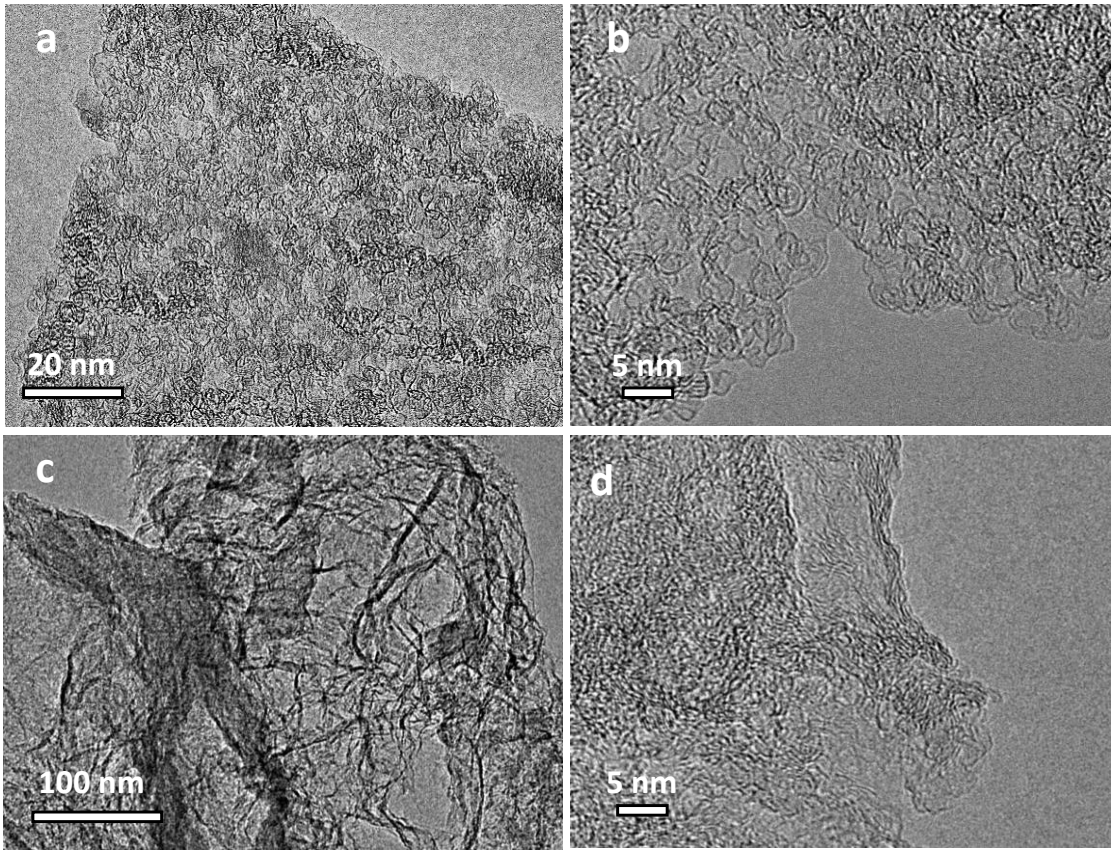

Figure S1. TEM images of (a,b) N,P-FC and (c,d) N,P-GC at different magnifications.

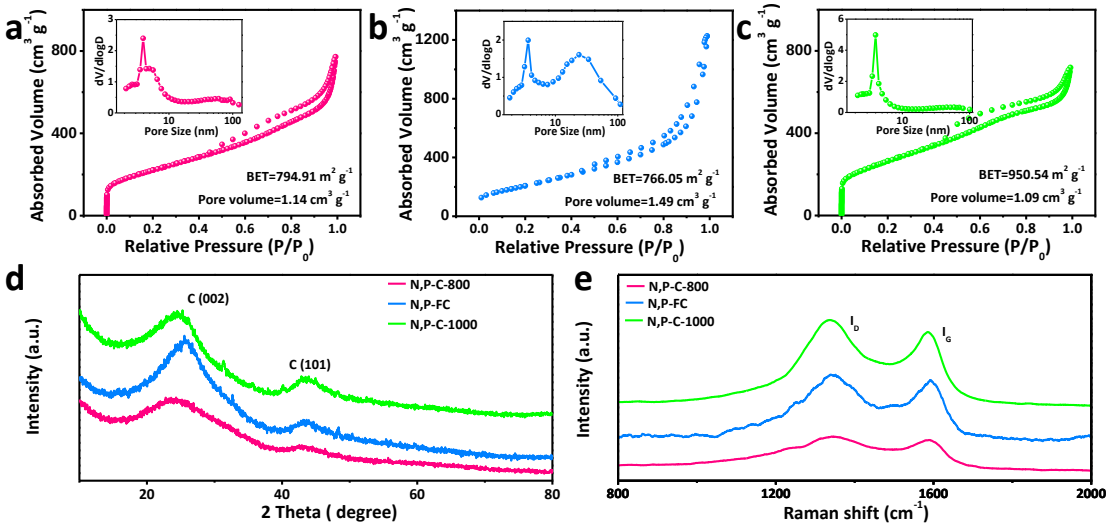

Figure S2. (a-c) N_2 adsorption/desorption isotherms of N,P-C-800, N,P-FC, N,P-C-1000, inset is pore size distribution of the N,P-C-800, N,P-FC, N,P-C-1000. (d) XRD pattern of of N,P-CN-800, N,P-FC, N,P-CN-1000. (e) Raman spectrum of N,P-C-800, N,P-FC, N,P-C-1000.

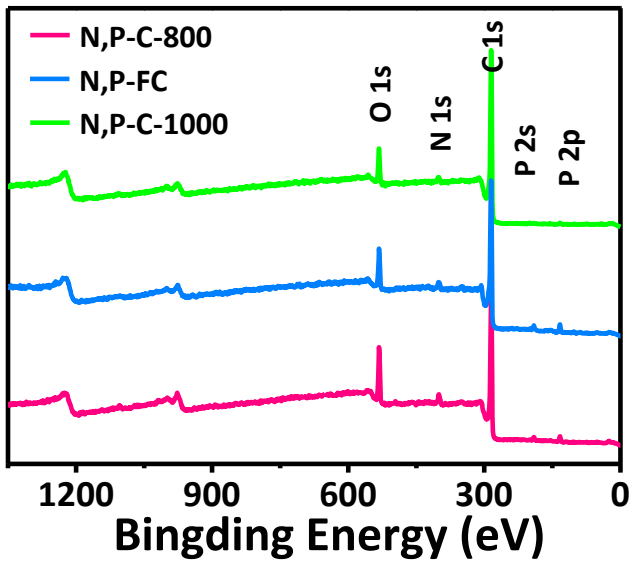

Figure S3. XPS spectrum of N,P-C-800, N,P-FC, N,P-C-1000.

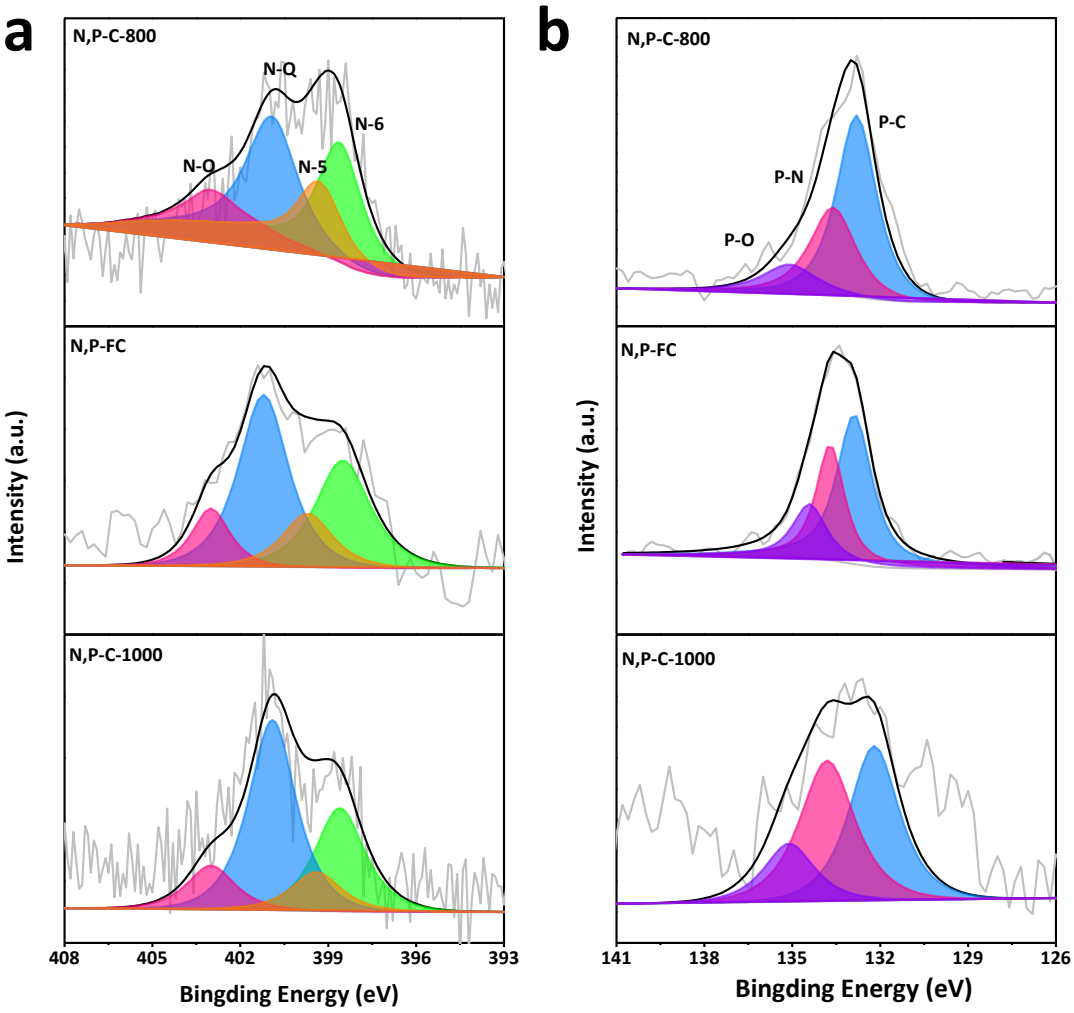

Figure S4. (a) High-resolution N 1s spectrum of N,P-C-800, N,P-FC, N,P-C-1000. (b) High-resolution P 2p spectrum of N,P-C-800, N,P-FC, N,P-C-1000.

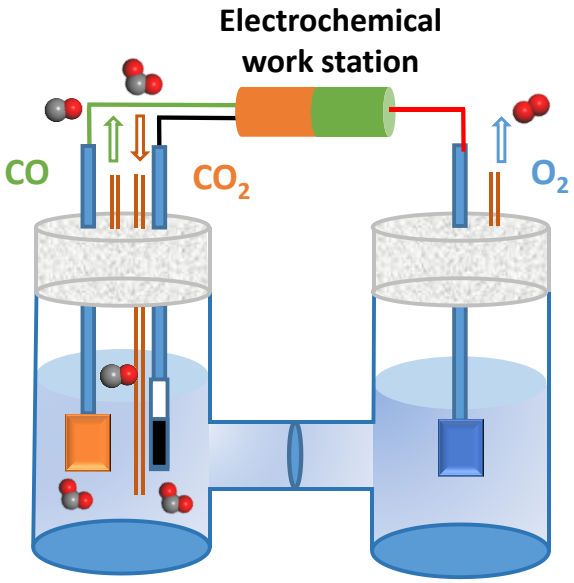

Figure S5. Electrolytic device schematic.

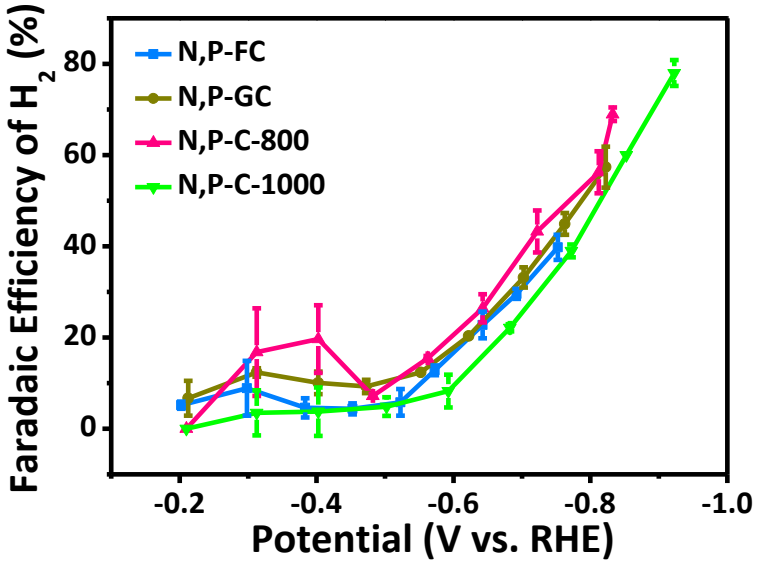

Figure S6. Faradaic efficiencies for H_2 production at different applied potentials.

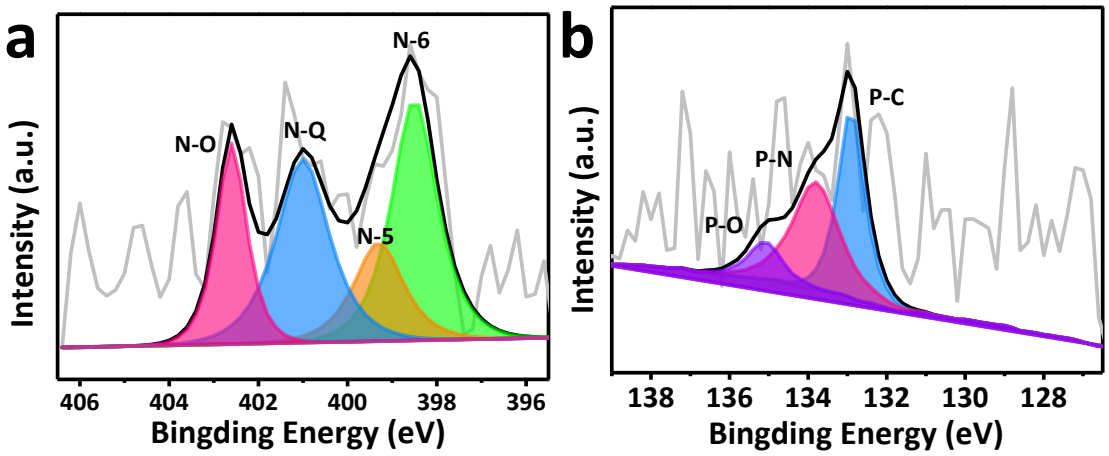

Figure S7. (a) High-resolution N 1s spectrum of the N,P-FC after stability test. (b) High-resolution P 2p spectrum of the N,P-FC after stability test.

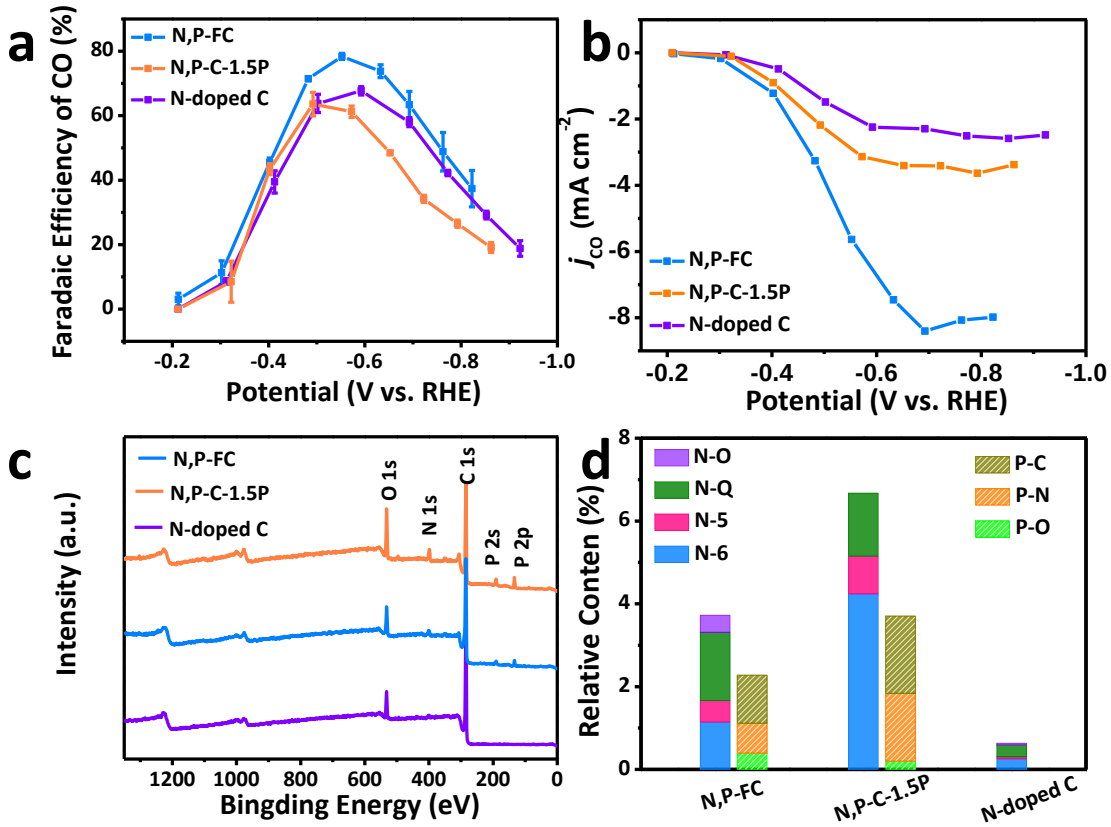

Figure S8. (a) Faradaic efficiencies for CO production at different applied potentials for N,P-FC, N,P-C-1.5P and N-doped C. (b) Partial current densities of CO N,P-FC, N,P-C-1.5P and N-doped C catalysts derived by corresponding potential-dependent FE data. (c) XPS spectrum of N,P-FC, N,P-C-1.5P and N-doped C, (d) Distribution of pyridinic-N, pyrrolic-N, graphitic-N, pyridinic $N^+–O^-$ obtained from the N 1s spectra and P-C, P-N, P-O obtained from the P 2p spectra of of N,P-FC, N,P-C-1.5P and N-doped C.

With the goal of investigating the role of P content in CO_2 reduction activity, we prepared samples without P (N-doped C) and samples with 1.5 times P (N, P-C-1.5P) as a control experiment, and compared their CO_2 reduction performance (Figure S8 and S9). It is obvious that addition of P could improve the properties of CO_2 reduction reaction. N,P-FC shows larger FE in each applied potential comparing with the sample without P. However, when the amount of P was increased to 1.5 times, it has an apparent drop in faradaic efficiency and only peaked at 63% at -0.5 V. Moreover, we also calculated the CO partial current density of three materials as shown in Figure S8b. The N,P-FC sample possessed outstanding current density among three materials. N-doped C showed larger faradaic efficiency than N,P-C-1.5P while its current density was quite small than the latter. These

results indicate that P plays a critical role in increasing current density during CO_2 reduction.

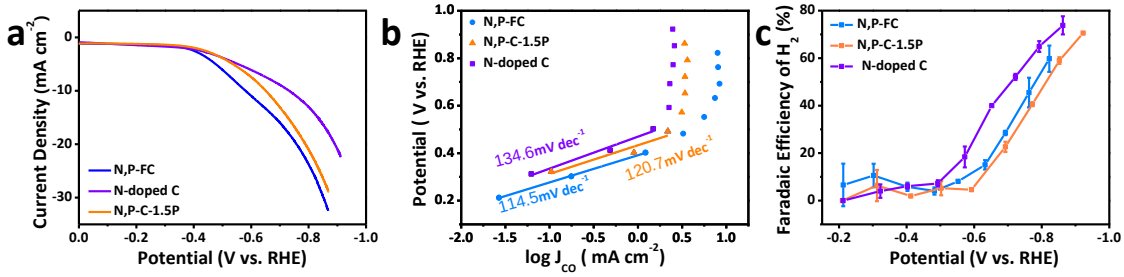

Figure S9. (a) Linear sweep voltammetric curves carried out in the CO_2-saturated 0.5 M $NaHCO_3$ aqueous solution for N,P-FC, N,P-C-1.5P and N-doped C. (b) Tafel plots of N,P-FC, N,P-C-1.5P and N-doped C electrodes for CO_2 reduction. (c) Faradaic efficiencies for H_2 production at different applied potentials.

To gain insight into the chemical origin of catalytic activity for electrochemical CO_2 reduction in N-doped C, N,P-FC and N, P-C-1.5P, XPS was used to probe the chemical state and coordination structure of this catalyst. The XPS survey spectra of the N,P-FC exhibit the presence of peaks corresponding to C, N, O, and P in the desired stoichiometric ratios, N-doped C showed no presence of a P peak, while N, P-C-1.5P showed a high P atomic ratio of up to 3.7 at.%, all this result indicating successful synthesis of these samples (Figure S8c). As shown in Figure S8d, S10, S11 and Table S3-S6, combined with XPS content and catalytic performance, the following conclusions can be obtained: i) the total contents of P and N have a linear relationship, the P content decreases, and the corresponding N content also decreases, when the P content decreases to 0, the N content value remains 0.61%. We speculate that due to the reaction of phytic acid with dicyandiamide to form macromolecules, the small molecules of dicyandiamide are less volatile during high-temperature carbonization, thereby increasing the N content. ii) When the P content is 1.5 times of the original, the overall N, P content increases due to the increase of the P content, but the catalytic activity decreases. We suspect that is due to successively generated P-doped defected sites destroys the original sp^2-network. iii) When P is absent, the N content is greatly reduced, and the catalytic activity is also reduced. This indicates that co-doping of catalyst improved the catalytic activity of material.

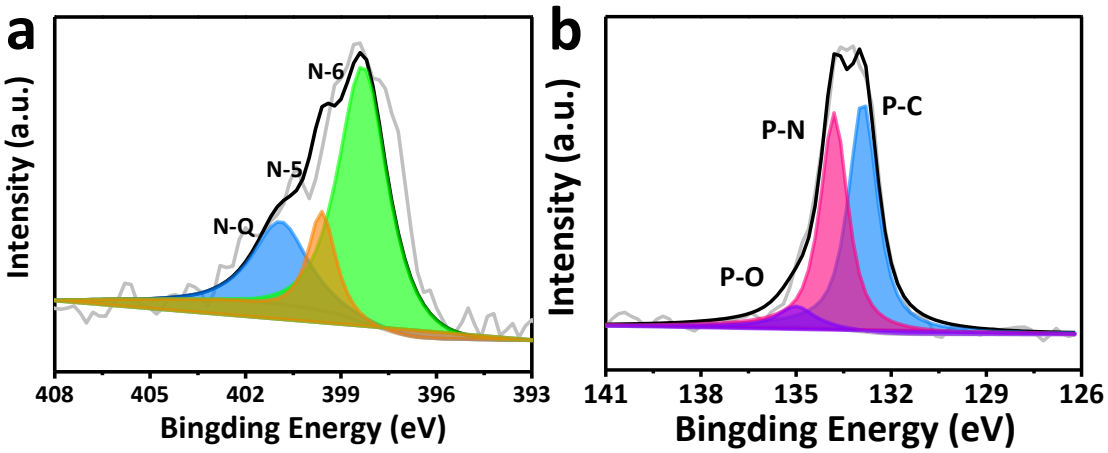

Figure S10. (a) High-resolution N 1s spectrum of the N,P-C-1. (b) High-resolution P 2p spectrum of the N,P-C-1.5P.

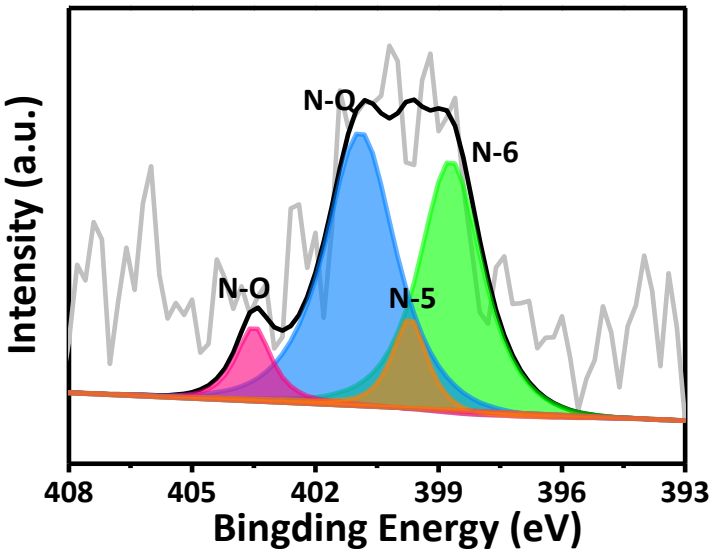

Figure S11. High-resolution N 1s spectrum of N-doped C.

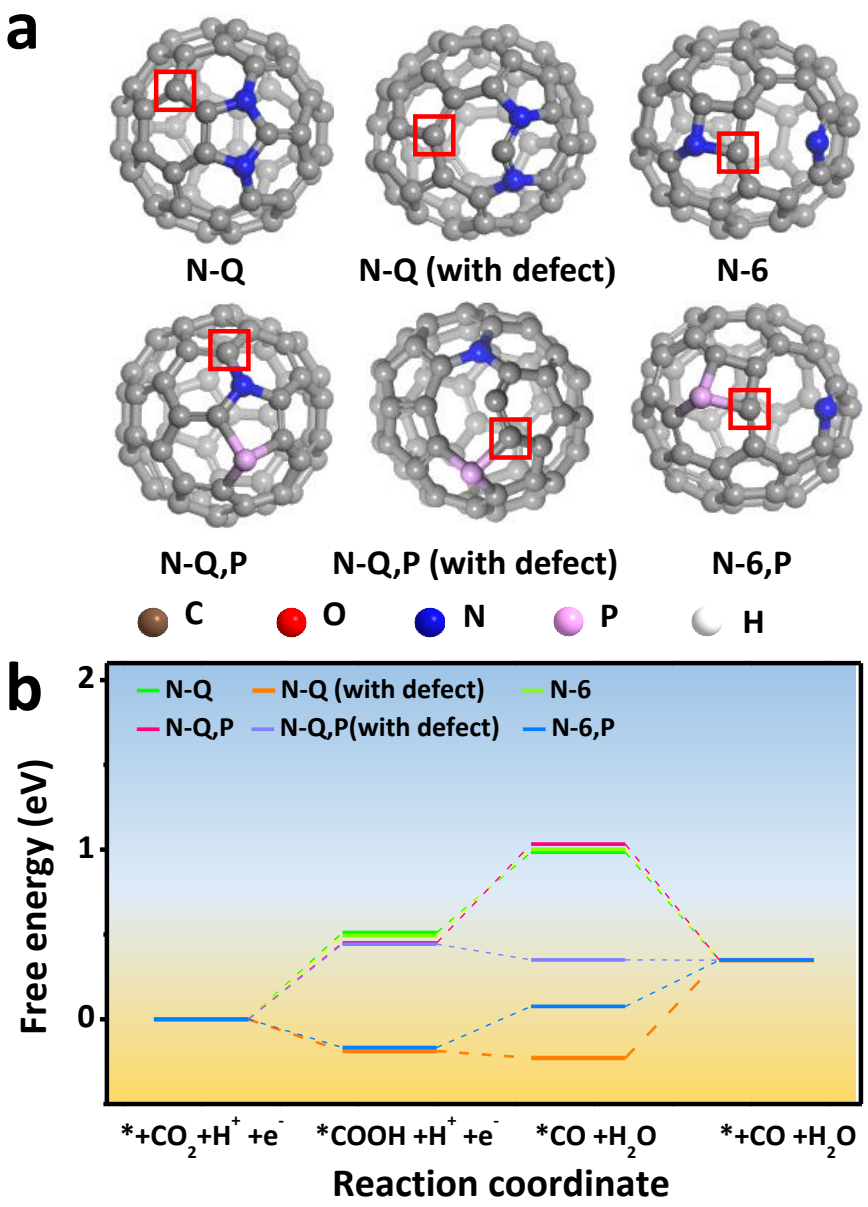

Figure S12. DFT modelling for CO_2 reduction reaction on N,P-FC. (a) Six types of active sites (Graphite-N, Graphite-N (with defect), Pyridine-N (with defect), Graphite-N,P, Graphite-N,P (with defect), Pyridine-N,P (with defect)) in the fullerenes model. (b) Free energy diagram of CO_2 reduction reaction to CO on N,P-FC (with fullerenes model).

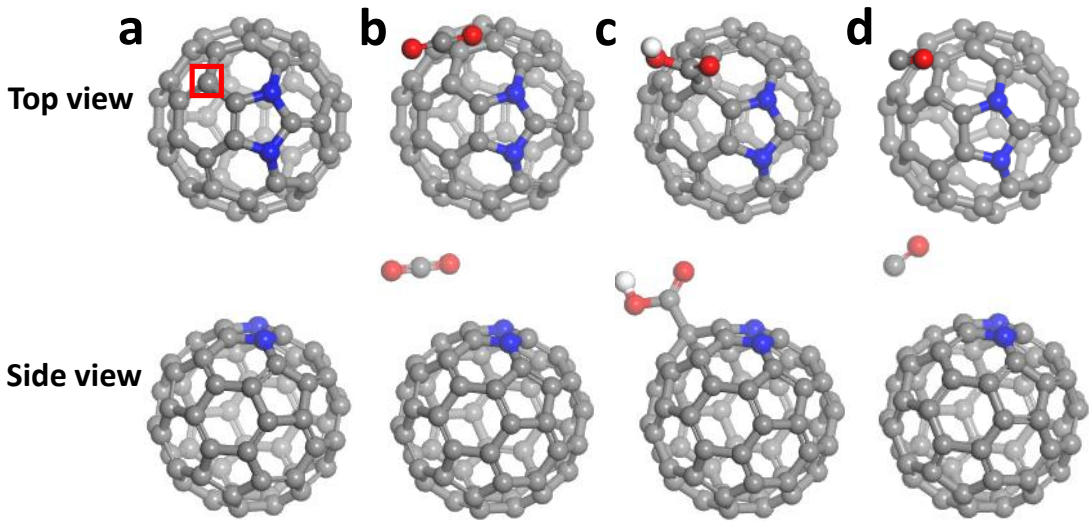

Figure S13. Energetically favorable structures for elementarysteps of CO_2 reduction on N-Q configuration of of fullerene model.

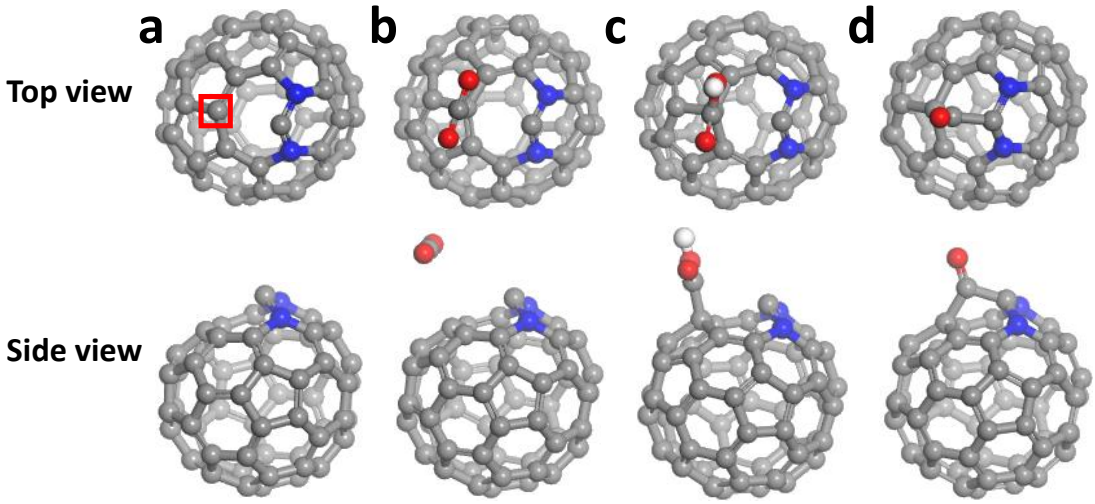

Figure S14. Energetically favorable structures for elementarysteps of CO_2 reduction on N-Q configuration(with defect) of of fullerene model.

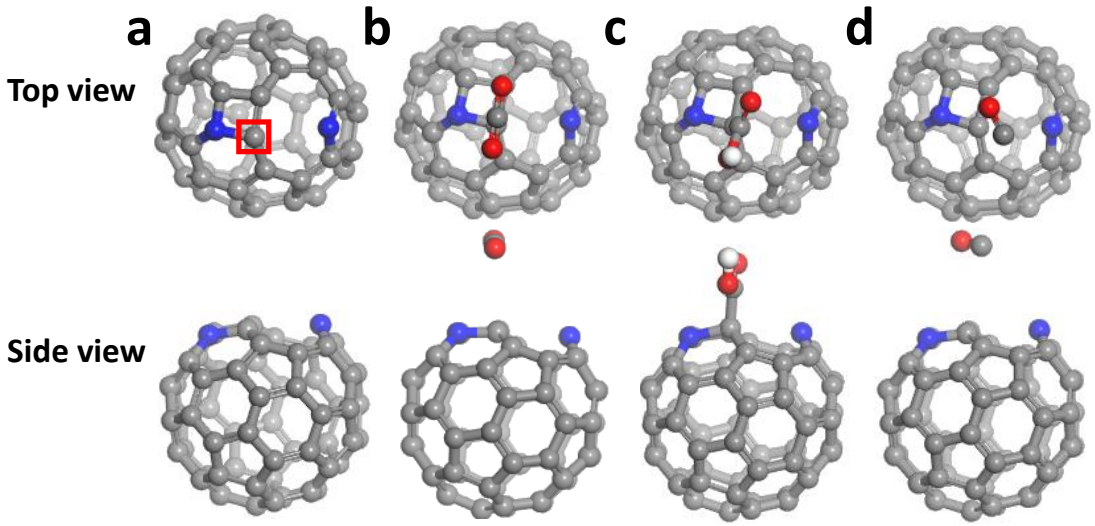

Figure S15. Energetically favorable structures for elementarysteps of CO_2 reduction on N-6 configuration of of fullerene model.

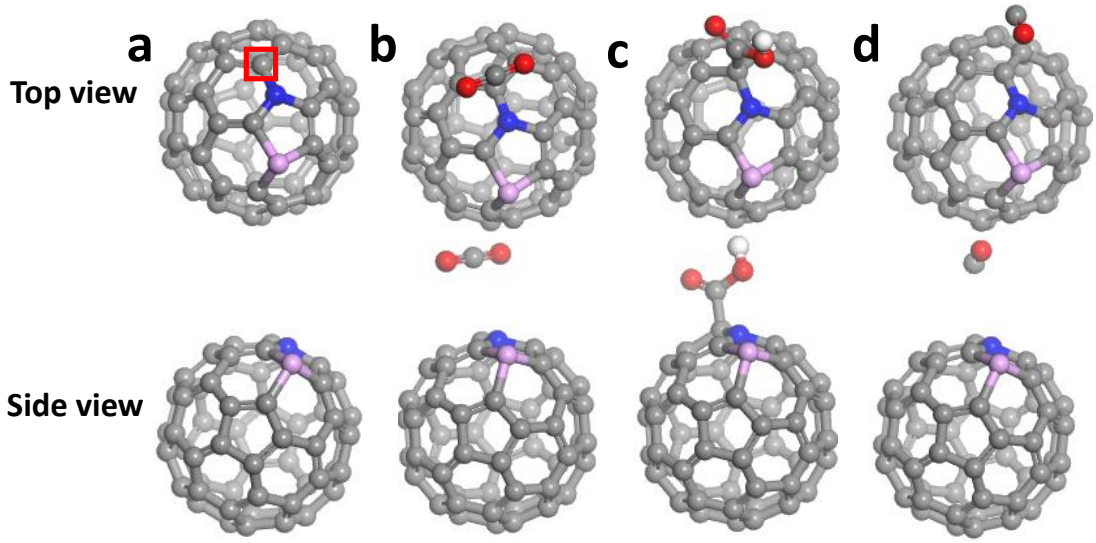

Figure S16. Energetically favorable structures for elementarysteps of CO_2 reduction on N-Q,P configuration of fullerene model.

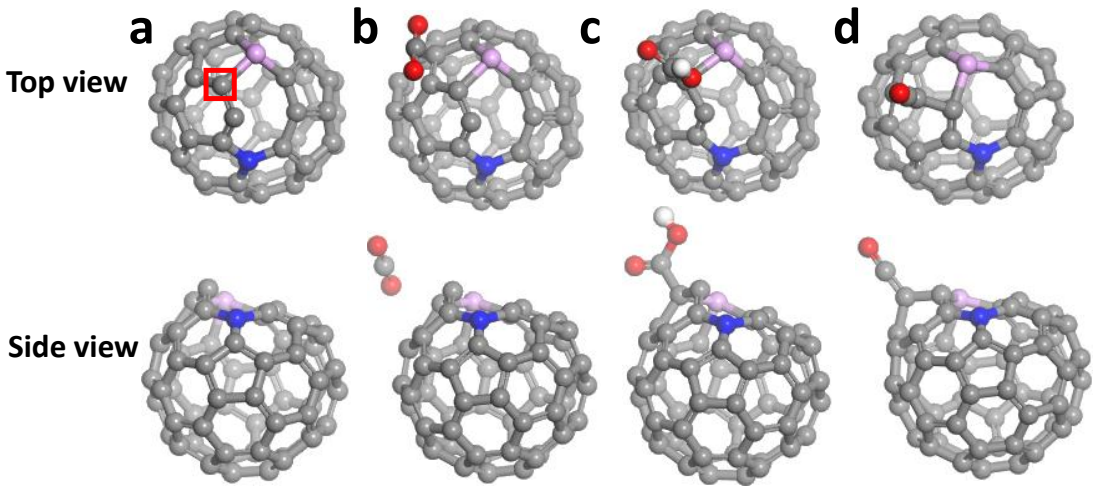

Figure S17. Energetically favorable structures for elementarysteps of CO_2 reduction on N-Q,P configuration (with defect) of fullerene model.

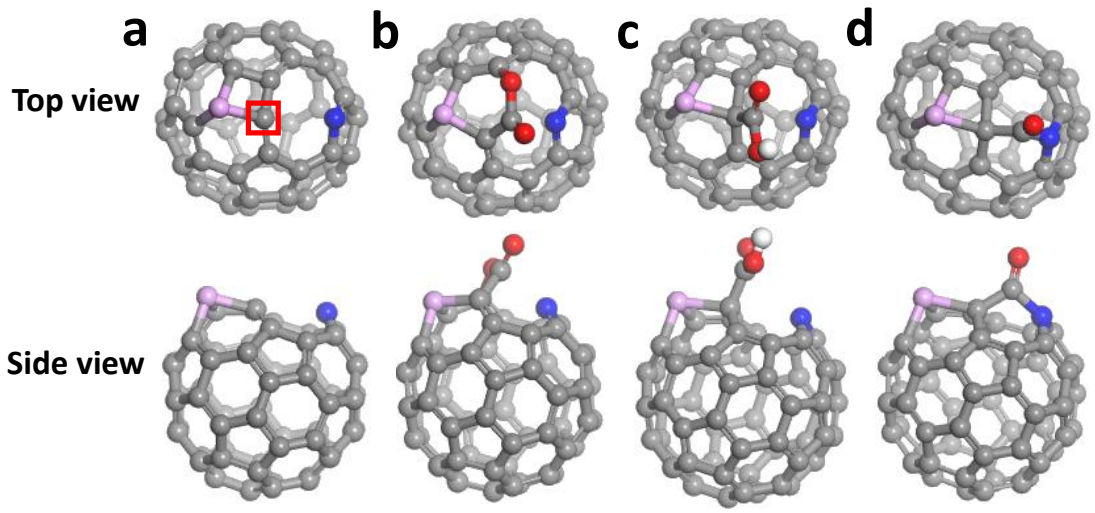

Figure S18. Energetically favorable structures for elementarysteps of CO_2 reduction on N-6,P configuration of fullerene model.

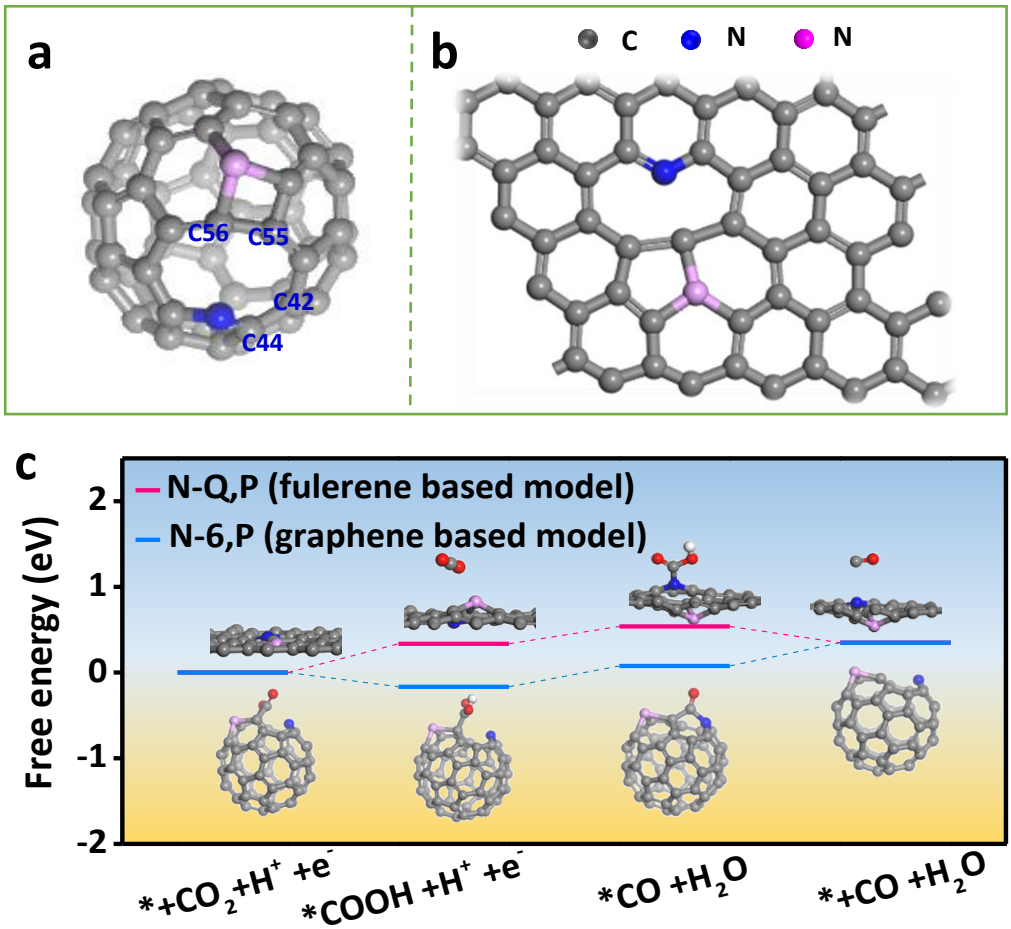

Figure S19. (a,b) DFT modelling for CO_2 reduction reaction on N,P-FC and N,P-GC. Two types of active sites in the fullerenes model and graphene model. (c) Free energy diagram of CO_2 reduction reaction to CO on N,P-FC and N,P-GC.

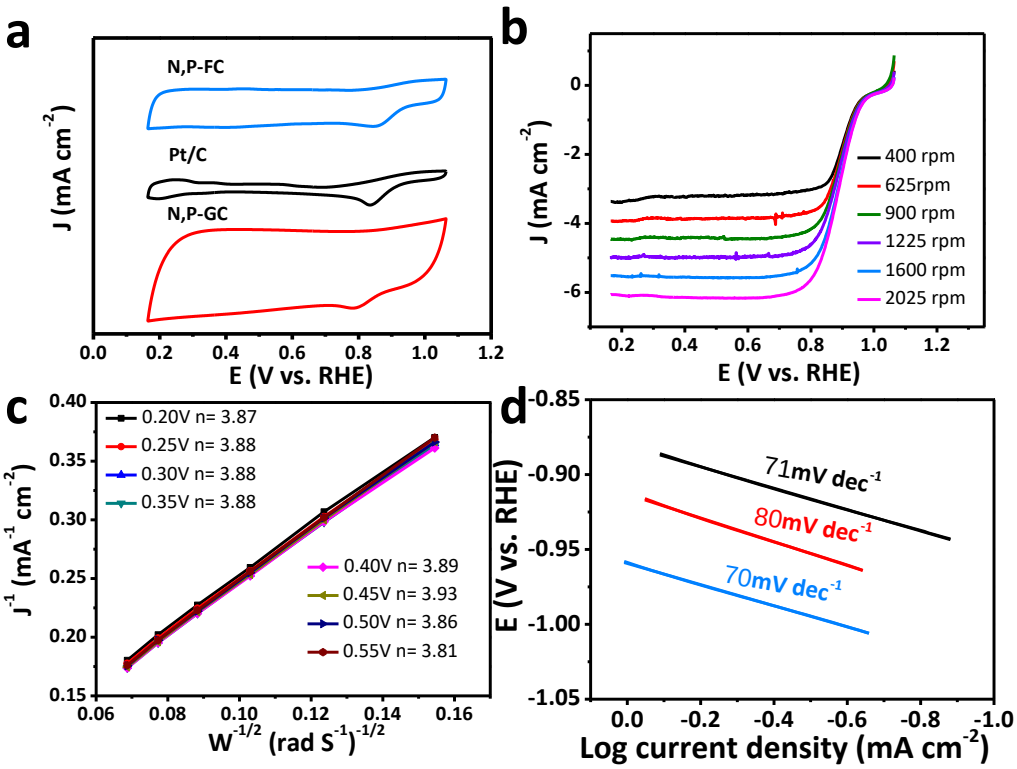

Figure S20. (a) CVs of N,P-FC, N,P-GC and Pt/C for ORR catalysis. (b) LSV curves at different rotation speeds from 400 to 1600 rpm for N,P-FC. (c) Corresponding K−L plots of N,P-FC. (d) The Tafel plots of N,P-FC, N,P-GC and Pt/C for ORR catalysis.

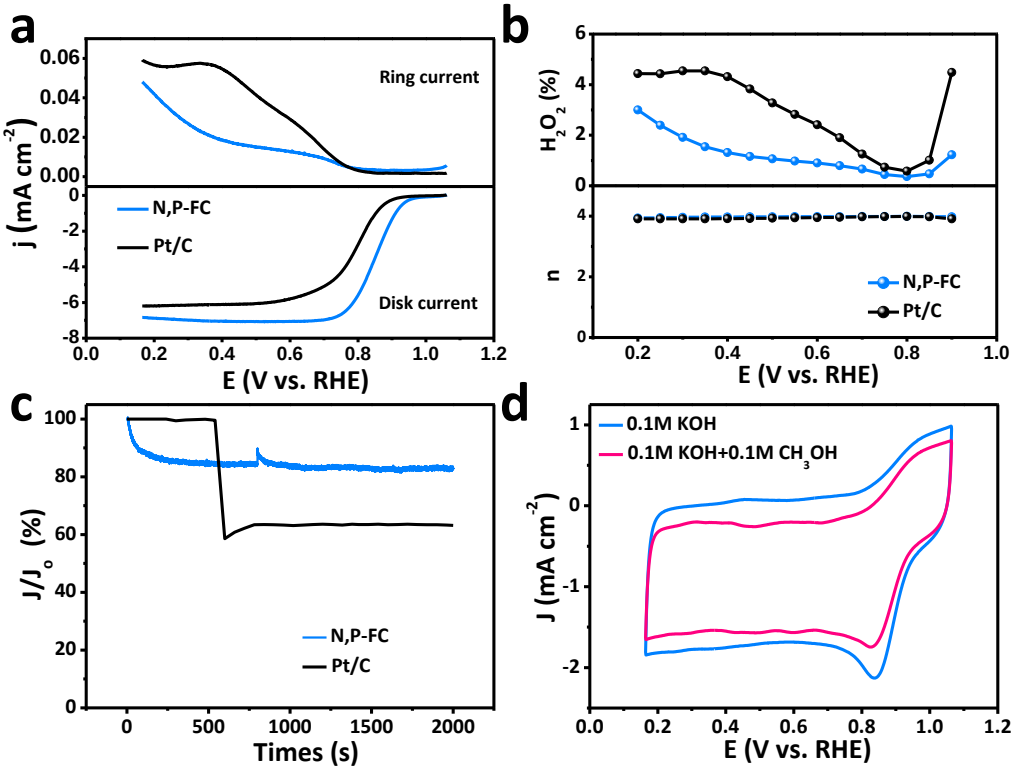

Figure S21. (a) RRDE voltammograms of N,P-FC in O_2-saturated solution at a scanning rate of 50 mV s^{-1} in 0.1 M KOH. (b) H_2O_2 yield and electron transfer number (n) in 0.1 M KOH solution. (c) Chronoamperometric response for N,P-FC and Pt/C electrode at 0.75 V (vs. RHE) after the introduction of 30.3 mL of CH_3OH into 219.7 mL of 0.1 M KOH solution. (d) LSV curves of 0.1 M KOH and 0.1 M CH_3OH of anti - methanol content of N,P-FC, the inset is CV curves of 0.1 M KOH and 0.1 M CH_3OH of anti - methanol content of N,P-FC.

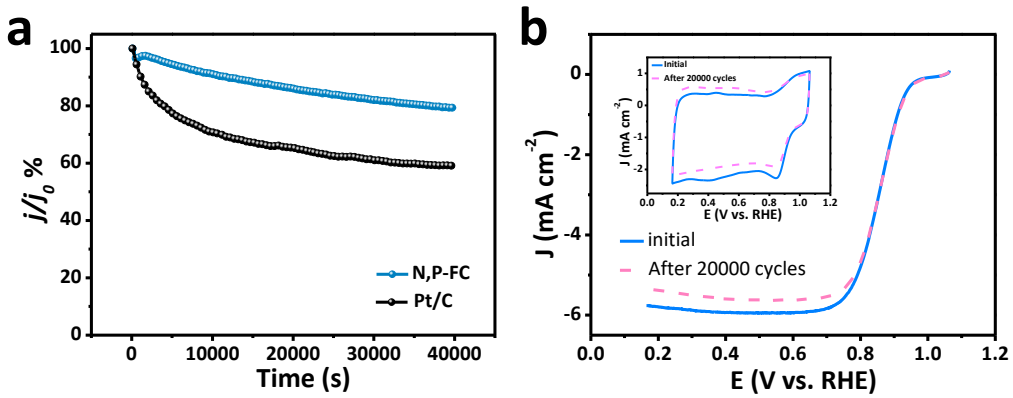

Figure S22. (a) The chronoamperometric response of N,P-FC and Pt/C in an O_2-saturated 0.1 M KOH solution at a potential of 0.8 V. (b) ORR polarization curves before and after 20000 potential cycles.

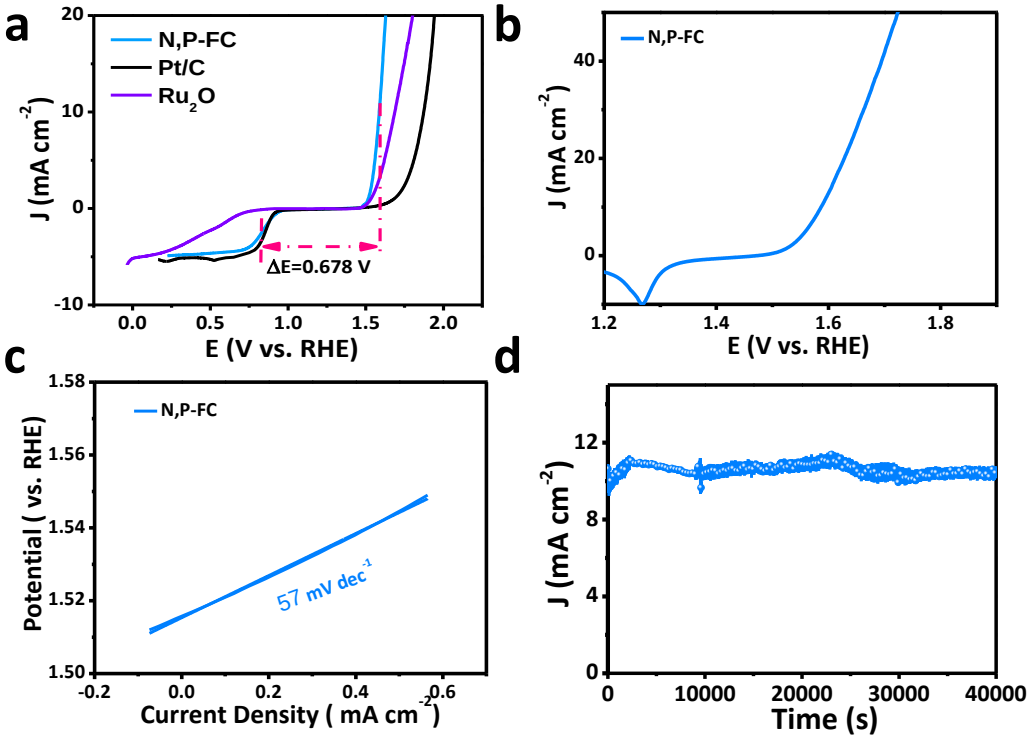

Figure S23. (a)LSV curves of different catalysts for both ORR and OER in 0.1 M KOH at 1600 rpm (scan rate 5 mV s^{-1}). (b) LSV curves of N,P-FC catalysts for OER in 1 M KOH. Scan rate: 5 mV s^{-1}. (c) Corresponding Tafel plots for OER catalysis. (d) Stability test of N,P-FC at 1.6 V in O_2-saturated 1 M KOH solution.

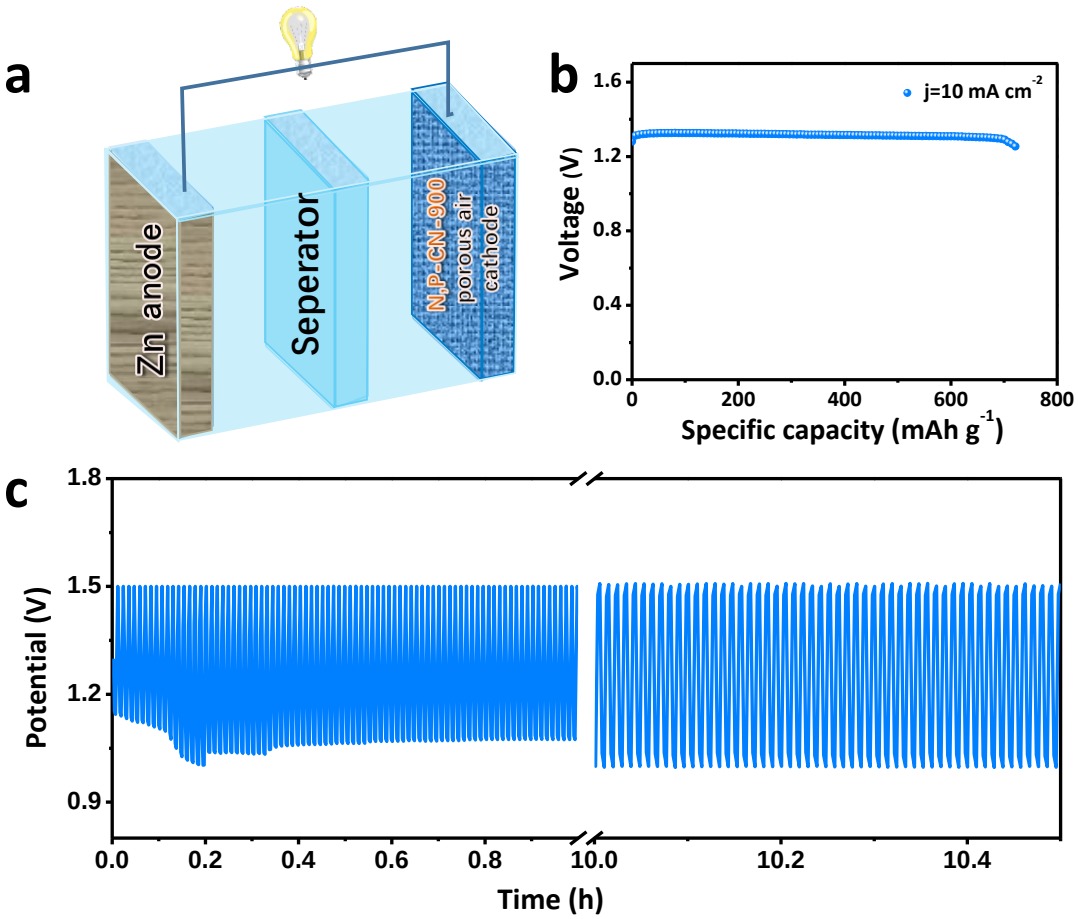

Figure S24. (a) Schematic representation of the rechargeable Zn-air battery. (b) Galvanostatic discharge curves of the primary Zn-air battery with N,P-FC as catalyst at 10mA cm^{-2} current densities. (c) Galvanostatic discharge-charge cycling curve at 1 mA cm^{-2} for the all-solid-state rechargeable Zn-air battery.

Table S1. Raman results analysis for the prepared samples.

Sample Name	**N,P-C-800**	**N,P-FC**	**N,P-C-1000**
I_D/I_G	**1.06**	**1.05**	**1.14**

Table S2. XPS results analysis for the prepared samples (at. %).

Sample Name	**C (at. %)**	**N (at. %)**	**O (at. %)**	**P (at. %)**
N,P-C-800	79.86	3.74	14.53	1.88
N,P-FC	83.15	3.72	10.14	2.27
N,P-C-1000	88.99	2.14	8.25	0.61
N,P-C-1.5P	73.84	6.67	15.44	3.7
N-doped C	89.61	0.63	9.75	0

Table S3. XPS results analysis of high-resolution N 1s spectrum for the prepared samples (at. %).

Sample Name	**pyridinic-N (at. %)**	**pyrrolic-N (at. %)**	**graphitic-N (at. %)**	**pyridinic N^+-O^- (at. %)**
N,P-C-800	33.33	20	36.67	10
N,P-FC	30.56	13.89	44.44	11.11
N,P-C-1000	28.37	10.64	49.64	11.35
N,P-C-1.5P	63.64	13.64	22.72	0
N-doped C	39.06	7.81	46.88	6.25

Table S4. XPS results analysis of high-resolution N 1s spectrum for the prepared samples (at. %) in the total sample.

Sample Name	**pyridinic-N (at. %)**	**pyrrolic-N (at. %)**	**graphitic-N (at. %)**	**pyridinic N^+-O^- (at. %)**
N,P-C-800	1.25	0.75	1.37	0.37
N,P-FC	1.14	0.52	1.65	0.41
N,P-C-1000	0.61	0.23	1.06	0.24
N,P-C-1.5P	4.24	0.91	1.52	0
N-doped C	0.25	0.05	0.29	0.04

Table S5. XPS results analysis of high-resolution P 2p spectrum for the prepared samples (at. %).

Sample Name	**P-O (at. %)**	**P-N (at. %)**	**P-C (at. %)**
N,P-C-800	10.39	31.17	58.44
N,P-FC	17.25	31.70	51.05
N,P-C-1000	15.78	42.11	42.11
N,P-C-1.5P	5.37	44.28	50.35
N-doped C	0	0	0

Table S6. XPS results analysis of high-resolution P 2p spectrum for the prepared samples (at. %) in the total sample.

Sample Name	**P-O (at. %)**	**P-N (at. %)**	**P-C (at. %)**
N,P-C-800	0.1953	0.5860	1.0987
N,P-FC	0.3916	0.7196	1.1589
N,P-C-1000	0.0962	0.2569	0.2569
N,P-C-1.5P	0.1987	1.638	1.8630
N-doped C	0	0	0

Table S7. Comparison of overpotentials and current density of CO formation at the maximum Faraday efficiency of N,P-FC with other electrocatalysts reported in the literature studies.

Catalysts	**Electrolyte**	**E_{app} (V vs. RHE)**	**J_{CO} (mA· cm^{-2})**	**Product /FEs**	**Reference**
N,P-FC	**0.5 M $NaHCO_3$**	**-0.52**	**~-8.5**	**CO/ 83.3%**	**This work**
NG-800	0.1 M $KHCO_3$	−0.47	~-1.8	CO/ 85%	Nano Lett. 2016, 16, 466
NCNTs	0.1 M $KHCO_3$	-0.26	~-0.7	CO/ 80%	ACS Nano 9, 5, 5364
N-graphene	0.5 M $KHCO_3$	−0.84	~-4.0	CO/ 73%	Green Chem. 2016, 18, 3250
CN-H-CNT	0.1 M $KHCO_3$	-0.5	~-2.0	CO/ 88%	Adv. Energy Mater. 2017, 1701456
NCNT	0.1 M $KHCO_3$	-1.05	~-2.5	CO/ 80%	Angew. Chem. Int. Ed. 2015, 54, 13701
Fe/NG-750	0.1 M $KHCO_3$	−0.57	~-2.6	CO/ 80%	Adv. Energy Mater. 2018, 1703487

Table S8. Reaction energetics for CO_2 reduction reaction to CO processes during CO_2RR.

	fullerenes model						**graphene model**
	N-Q	**N-Q (with defect)**	**N-6**	**N-Q,P**	**N-Q,P (with defect)**	**N-6,P**	**N-6,P**
$*+CO_2+H^+ +e^-$	0	0	0	0	0	0	0
$*COOH +H^+ +e^-$	0.511	-0.187	0.494	0.45	0.443	-0.167	0.335
$*CO +H_2O$	0.985	-0.229	1.001	1.033	0.35	0.076	0.538
$*+CO +H_2O$	0.349	0.349	0.349	0.349	0.349	0.349	0.349

Table S9. Reaction energetics for the 4-elctron transfer processes during ORR. ΔG, free energy change at T=298 K and pH=13.

Elementary Reactions	**C next to N U=0 V**	**C next to P U= 0 V**	**C next to N U = 0.726**
$O_2(g) + * \Rightarrow O_2*$	4.92	4.92	2.0136
$O_2* + H_2O(l) + e^- \Rightarrow OOH* + OH^-$	3.8808	3.5428	1.701
$OOH* + e^- \Rightarrow O* + OH^-$	1.68841	1.00454	0.23521
$O* + H_2O(l) + e^- \Rightarrow OH* + OH^-$	0.7266	0.0361	0
$OH* + e^- \Rightarrow OH^- + *$	0	0	0

Table S10. Total energies of fullerene models (N,P-FC) and O*, OH*, OOH* species on different sites.

	C next to P	**C next to N**
E(*)	-516.9098257	-516.9098257
E(OH*)	-528.0339079	-527.3434255
E(O*)	523.3370891	522.6532178
E(OOH*)	-531.9060675	-531.5679765

Table S11. Total energies (E) of H_2O and H_2 from DFT and Zero point energy (ZPE) corrections and entropic contributions (TS) to the free energies.

Species	E	ZPE	TS
H_2O (0.035bar)	-14.219	0.56	0.67
H_2	-0.674	0.27	0.41
O*	-	0.084	0.05
OH*	-	0.386	0.07
OOH*	-	0.457	0.16

The gas phase values were from Ref. 18, while the values for the adsorbed species were taken from DFT calculations. Gas phase H_2O at 0.035 bar was used as the reference state because at this pressure gas phase H_2O is in equilibrium with liquid water at 300 K. The same values for the adsorbed species for all the models were used, as vibrational frequencies have been found to depend much less on the surface than the bond strength.

Table S12. Frequencies of adsorbed species.

Adsorbed Species	Frequency (cm^{-1})
O*	185.7, 293.9, 872.8
OH*	256.4, 265.1, 290.5, 575.0, 1170.7, 3666.8
OOH*	53.2, 151.8, 264.6, 309.1, 321.8, 558.3, 781.0, 1285.2, 3647.6

Table S13. Comparison sample of the N,P-FC electrocatalysts.

Catalysts	Onset Potential (V)	$E_{½}$ (V vs. RHE)	J_L ($mA\ cm^{-2}$)
N,P-FC	0.959	0.910	-5.41
N,P-GC	0.912	0.841	-5.78
Pt/C	0.878	0.831	-5.54

Table S14. Comparison of ORR catalystic activity between N,P-FC product and other well-developed Carbon based ORR electrocatalysts in alkali solution.

Catalysts	**E_{onset} (V)**	**$E_{1/2}$(V)**	**$J_{limiting}$ (mA cm^{-2})**	**Reference**
N,P-FC	**0.959**	**0.910**	**5.41**	**This work**
Pt/C	**0.878**	**0.831**	**5.54**	**This work**
SHG	1.01	0.87	5.10	Adv. Mater. 2017, 29, 1604942
NDGs-800	0.98	0.85	5.60	ACS Energy Lett. 2018, 3, 1183
Co_2P/CoN-in-NCNTs	0.96	0.85	5.01	Adv. Funct. Mater. 2018, 28, 1805641
Co-P,N-CNT	0.916	0.803	5.99	Chem. Commun. 2017, 53, 9862
Fe-ISAs/CN	-	0.900	-	Angew. Chem. Int. Ed. 2017, 56, 1
FeNC-S-FexC/Fe	1.05	0.873	5.45	Adv. Mater. 2018, 30, 1804504
P,S-CNS	0.97 V	0.870	7.14	ACS Nano 2017, 11, 347
Co–Nx/C NRA	-	0.877	-	Adv. Funct. Mater. 2018, 28, 1704638
Fe2-Z8-C	0.985	0.871	-	Angew. Chem. Int. Ed. 2018, 57,1204
N-Fe-CNT/CNP	-	0.870	-	Nat. Commun. 2013, 4:1922
S-C_2N	0.98	0.880	6.60	ACS Nano 2018, 12, 596
NPMC-1000	0.94	0.850	4.20	Nat. Nanotechnol. 2015, 10, 444

References

1. Q. Liu, Y. Wang, L. Dai and J. Yao, *Adv. Mater.*, 2016, **28**, 3000-3006.
2. J. Zhang, L. Qu, G. Shi, J. Liu, J. Chen and L. Dai, *Angew Chem. Int. Ed.*, 2016, **55**, 2230-2234.
3. W. Niu, L. Li, N. Wang, S. Zeng, J. Liu, D. Zhao and S. Chen, *J. Mater. Chem. A*, 2016, **4**, 10820-10827.
4. Z. Cheng, Q. Fu, C. Li, X. Wang, J. Gao, M. Ye, Y. Zhao, L. Dong, H. Luo and L. Qu, *J. Mater. Chem. A*, 2016, **4**, 18240-18247.
5. M. Wang, T. Qian, S. Liu, J. Zhou and C. Yan, *ACS Appl. Mater. Interfaces*, 2017, **9**, 21216-21224.
6. X. Wang, X. Lu, B. Liu, D. Chen, Y. Tong and G. Shen, *Adv. Mater.*, 2014, **26**, 4763-4782.
7. P. E. Blochl, *Phys. Rev. B*, 1994, **50**, 17953-17979.
8. J. P. Perdew, K. Burke and M. Ernzerhof, *Phys. Rev. Lett.*, 1996, **77**, 3865-3868.
9. G. K. a. J. Furthmüller, *Phys. Rev. B,* 1996, **54**, 11169-11186.
10. G. K. a. D. Joubert, *Phys. Rev. B*, 1999, **59**, 1758-1775.
11. F. Gao, G. L. Zhao, S. Yang and J. J. Spivey, *J. Am. Chem. Soc.*, 2013, **135**, 3315-3318.
12. S. Grimme, J. Antony, S. Ehrlich and H. Krieg, *J. Chem. Phys.*, 2010, **132**, 154104.
13. A. A. Peterson, F. Abild-Pedersen, F. Studt, J. Rossmeisl and J. K. Norskov, *Energ. Environ. Sci.*, 2010, **3**, 1311-1315.
14. J. K. Norskov, J. Rossmeisl, A. Logadottir, L. Lindqvist, J. R. Kitchin, T. Bligaard and H. Jonsson, *J. Phys. Chem. B*, 2004, **108**, 17886-17892.
15. W. Kohn and L. J. Sham, *Phys. Rev.,* 1965*,* **140***,* A1133-1138*.*
16. J. P. Perdew and Y. Wang, *Phys. Rev., B* 1992, **45**, 13244-13249*.*
17. S. Grimme, *J. Comp. Chem.,* 2006, **27**, 1787-1799.
18. M. Li, L. Zhang, Q. Xu, J. Niu and Z. Xia, *J. Catal.*, 2014, **314**, 66-72.